International Research Journal of Multidisciplinary Scope (IRJMS), 2026; 7(2): 764-777 IRJMS

Original Article | ISSN (O): 2582-631X DOI: 10.47857/irjms.2026.v07i02.08248

Noise Mitigation of a 5-phase Field-oriented-controlled Permanent Magnet Synchronous Machine Drive System Using Kalman Filter-based Model-predictive-controller

Vivek Pahwa*

Department of Electrical and Electronics Engineering, University Institute of Engineering and Technology, Panjab University, Chandigarh, India. *Corresponding Author's Email: v1974pahwa@gmail.com

Abstract

The performance of advanced drive systems in most of the sophisticated motion control industries is compromised by inherent sensor noise, which, in extreme cases, may induce undesirable instability. This research investigates the application of a Kalman filter-based model predictive controller to attenuate noise generated by the mechanical speed sensor in a 5-phase field oriented controlled permanent magnet synchronous machine drive system. Comparative analysis with a proportional-integral-based controller reveals that the proposed method can potentially reduce both rotor speed and electromagnetic torque noise by approximately 75% respectively under steady-state conditions. And, stator current is reduced by 66% with proposed controller. Initial evaluations are conducted in an offline MATLAB/SIMULINK environment, a crucial procedural step. Despite yielding accurate results, the substantial computational burden due to sequential processing, estimated at 1900 (approx.), poses challenges for its practical implementation. To address this limitation, the offline models are converted to online models with a Field Programmable Gate Array based rewritable OPAL-RT [4510] real time simulator with its enhanced parallel processing capability. This cost-effective methodology not only substantiates the research findings by eliminating system-specific and exorbitant experimental configurations but also augments the practicality of real world applications by diminishing the computational burden to the requisite value of 1.

Keywords: 5-phase PMSM, Drive System, Field Oriented Control, MPC, Real-time Simulation.

Introduction

Permanent magnet synchronous machines (PMSMs) offer significant advantages over conventional electrical machines such as DC and three-phase induction motors: superior torque-to-weight ratio, improved speed control performance and enhanced efficiency. These advantages have rendered PMSMs as the preferred choice in advanced industrial motion control applications (1). The implementation of field-oriented-control (FOC) techniques has also substantially improved the dynamic performance of PMSM drive systems (2, 3). Consequently, the FOC approach is selected for the dynamic control of this machine, referred to as the FOCPMSM drive system. The mechanical speed sensor plays a crucial role in abc-dq and dq-abc transformations of FOC operation (4). Due to harsh environmental conditions and continuous vibrations, the sensor performance deteriorates over time, resulting in undesirable noise (5). If not addressed appropriately, this may cause the drive system to enter an unstable region, which is a highly undesirable condition in modern industry. The electromagnetic forces also cause noise and vibration in PMSMs (6). To address this issue, several techniques have been developed for noise suppression and sensor-related improvements. One such method is rotor-step skewing, which can be implemented as either straight skewing or zigzag skewing. Rotor-step zigzag skewing has been found to be more effective in restraining electromagnetic vibration compared to straight skewing, especially when considering the elastoplasticity of the stator material (7). In another study, it has been shown that the rotor position errors can introduce extra side-band frequency harmonics to the current and electromagnetic force, leading to more abundant noise harmonics (8). These mechanical design improvement techniques can be implemented during development stages and works for noise suppression only. From a control perspective, the proportional–integral (PI) controller remains the

(Received 17th September 2025; Accepted 06th March 2026; Published 13th April 2026)

most widely used strategy due to its simplicity and ease of implementation (9). Nevertheless, PI control lacks inherent mechanisms for disturbance estimation and noise suppression, resulting in compromised performance in the presence of sensor noise and parameter uncertainties (10). Achieving simultaneous dynamic performance enhancement and effective noise mitigation thus remains a significant challenge in PMSM drive systems.

In this context, an extended state observer (ESO) based active disturbance rejection control (ADRC) strategy has been proposed to address the limitations of the conventional PI control approach (11). Although efforts have been made to enhance this ADRC strategy through cascaded ESO, nonlinear ESO, a combination of ESO and finite time technique and adaptive switching ESO but, these iterations demonstrated greater efficacy in mitigating disturbances rather than noise (12-15). Furthermore, these enhancements result in increased order and complexity, consequently diminishing reliability. Moreover, these modifications are system-specific.

In contemporary systems, integrated features such as future-state predictions, advanced error reduction algorithms with aggressive control inputs and sophisticated and measurement noise mitigation techniques render the model predictive control (MPC) approach superior in comparison to the aforementioned ADRC techniques. As a fundamental component of MPC, the observer plays a crucial role in accurately predicting states for effective control. Numerous observers, such as the Luenberger-based observer, the combination of stator current and disturbance observer and parallel ESO, were applied to achieve the objectives of this work (16-18). Recently, augmented extended nonlinear state observer has been applied on PMSM drive system for mitigation of noise from its speed sensor (19). However, the effect of noise in torque has not been addressed. Moreover, these approaches increase the system's complexity.

An optimal observer, namely the Kalman filters (KF), which observes states accurately, is capable of effectively suppressing noise. Moreover, it is most suitable for the MPC structure. Therefore, a Kalman filter (KF) based Model Predictive Control (MPC) strategy has been applied to Permanent Magnet Synchronous Motor (PMSM) drive systems, which effectively suppresses sensor noise (20). Furthermore, the machine's dynamics have been improved with direct-torque-control (DTC). However, the DTC technique produces more current and torque ripples in comparison to Field-Oriented Control (FOC) and the machine utilized is three-phase in nature (21).

Although three-phase PMSM is employed in numerous applications, its five-phase counterpart is rapidly gaining prominence in modern motion control systems, particularly in the automotive industry, due to its compactness, higher torque density and fault-tolerant capabilities (22, 23). However, this highly non-linear machine exhibits more complex dynamics due to complicated coupling (24). Consequently, controller design for this machine presents a significant challenge.

The majority of the aforementioned research concerning the development and comprehensive analysis of drives and their control strategies has been conducted using offline MATLAB/SIMULINK platform. While this environment is essential for the initial development of drive systems, its inconsistent timing and sequential execution of simulations render it unsuitable for real-time implementations. In contrast, the consistent timing and parallel processing capabilities of the OPAL-RT real-time simulator (online environment) facilitate rapid prototyping, testing of control algorithms and real-time implementation (25 -28) .

From the above discussion, it is evident that no existing work simultaneously addresses mechanical speed sensor noise suppression, dynamic performance enhancement, five-phase FOC-PMSM nonlinear decoupling and real-time validation within a unified control framework.

Accordingly, the primary objective of this research is to develop and experimentally validate a Kalman Filter-based Model Predictive Control (KF-MPC) strategy for mitigating mechanical speed sensor noise and improving the dynamic performance of a five-phase FOC-PMSM drive system.

The present work is structured around four specific objectives. First, a noise-aware state-space representation of a five-phase field-oriented controlled permanent magnet synchronous motor (FOC-PMSM) drive system is developed, ensuring suitability for model predictive control (MPC) implementation. Second, an optimal Kalman Filter (KF) is integrated within the MPC framework to achieve effective suppression of mechanical speed

sensor noise. Third, a comprehensive quantitative performance evaluation of the proposed KF–MPC scheme is conducted and bench-marked against a conventional proportional–integral (PI) controller under noisy operating conditions in an offline simulation environment. Finally, the real-time feasibility and control performance of the proposed controller are experimentally validated using an OPAL-RT 4510 real-time digital simulator. By achieving these objectives, the proposed approach provides a theoretically sound and practically deployable solution for noise-resilient, high-performance control of five-phase PMSM drive systems.

Methodology

This section presents the mathematical modelling of a 5-phase field-oriented-controlled permanent magnet synchronous machine drive system (including sensor noise) and its model-predictive-controller. The schematic diagram representation of this whole system is given in figure 1 and the control of 5-phase FOCPMSM can be understood in the following way. The speed output including noise is taken from speed sensor and fed to the model-predictive-controller. The controller compares this input speed including noise with reference speed and gives the reference q-axis current, which is being fed to transformation block. The block transforms the reference currents into stationary currents and these currents are converted into reference 5-phase currents. Then, these reference currents are compared with actual 5-phase machine currents with a hysteresis controller. The generated gate signals are given to current controlled voltage source inverter, which generates the appropriate voltage signals to be applied to the 5-phase PMSM.

The stator voltage (Equations [1-4]) and flux linkage Equations [5-8] of 5-phase FOCPMSM in d_1-q_1-d_2-q_2 reference frame are given as (25):

$$v_{d1} = r_s i_{d1} - \omega\varphi_{q1} + \frac{d\,\varphi_{d1}}{dt} \quad [1]$$

$$v_{q1} = r_s i_{q1} - \omega\varphi_{d1} + \frac{d\,\varphi_{q1}}{dt} \quad [2]$$

$$v_{d2} = r_s i_{d2} - 3\omega\varphi_{q2} + \frac{d\,\varphi_{d2}}{dt} \quad [3]$$

$$v_{q2} = r_s i_{q2} - 3\omega\varphi_{d2} + \frac{d\,\varphi_{q2}}{dt} \quad [4]$$

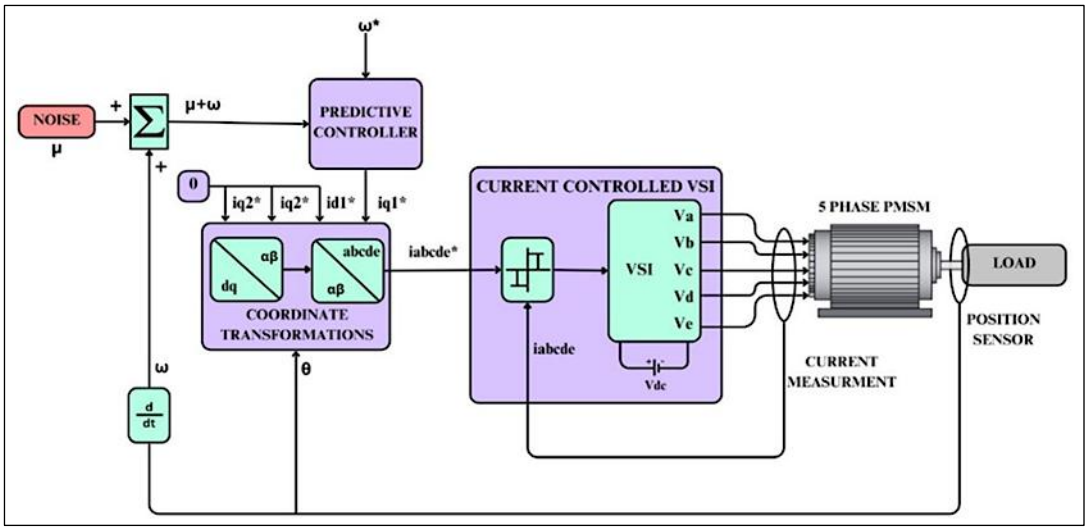

Figure 1: Model-predictive-controlled 5-phase FOCPMSM with Noise

Where,

$$\varphi_{d1} = Li_{d1} + \varphi_{m1} \quad [5]$$

$$\varphi_{q1} = Li_{q1} \quad [6]$$

$$\varphi_{d2} = Li_{d2} + \varphi_{m2} \quad [7]$$

$$\varphi_{q2} = Li_{q2} \quad [8]$$

Where, v_{d1}, v_{q1}, v_{d2} and v_{q2} are the applied stator voltages on the d_1-q_1-d_2-q_2 axis. And, i_{d1}, i_{q1}, i_{d2} and i_{q2} are the currents on the d_1-q_1-d_2-q_2 axis. The fluxes on d_1-q_1-d_2-q_2 axis are $\varphi_{d1}, \varphi_{q1}, \varphi_{d2}$ and φ_{q2}. The angular frequency (rad/sec) is given by ω. The stator resistance and inductance of the 5-phase PMSM is given by r_s and L respectively. The mutual fluxes are represented by φ_{m1} and φ_{m2}.

Further, the electro-magnetic torque, T_e developed by the 5-phase PMSM is given by Equation [9]:

$$T_e = \frac{5}{2}\frac{P}{2}\left(\varphi_{m1} i_{q1} + 3\varphi_{m2} i_{q2}\right) \quad [9]$$

The field-oriented-controlled operation of 3-phase PMSM is obtained by keeping $i_d \rightarrow 0$ in electro-magnetic torque Equation of this machine and, in the similar way, the FOC operation of a 5-phase PMSM drive system can be obtained by putting $i_{d1} = i_{d2} = i_{q2} \rightarrow 0$ in Equation [4, 9]. The electro-magnetic torque Equation [10] in terms of reference q-axis current, i_{q1}^* can be given as:

$$T_e = \frac{5}{2}\frac{P}{2}\left(\varphi_{m1} i_{q1}^*\right) \quad [10]$$

The Equations [11] and onwards have been derived on the basis of three-phase PMSM drive system given in and illustrated as (20):

$$J\frac{d\omega_m}{dt} = T_e - T_L - B_m\omega_m \quad [11]$$

$$\omega = \frac{P}{2}\omega_m \quad [12]$$

Where,

J= Moment of inertia, T_L= Applied load torque and ω_m= Mechanical angular frequency. And ω in Equation [12] is angular velocity (electrical) in rad/sec. Further, the Equation [11] can be rewritten as Equation [13], and then as Equation [14]:

$$\dot{\omega_m} = \left(-\frac{B_m}{J}\right)\omega_m + \left(-\frac{1}{J}\right)T_L + \left(\frac{K_1\varphi_{m1}}{J}\right)i_{q1}^* \quad [13]$$

$$\dot{\omega_m} = M_1\omega_m + M_2 T_L + M_3 i_{q1}^* \quad [14]$$

Where,

$$M_1 = \left(-\frac{B_m}{J}\right), M_2 = \left(-\frac{1}{J}\right) \text{ and } M_3 = \left(\frac{K_1\varphi_{m1}}{J}\right)$$

$$\dot{\theta} = \omega_m \quad [15]$$

Equation [15] gives the rate of change of angle. Further, the electro-dynamic system of the 5-phase FOCPMSM drive system shown in Figure 1, including the noise and measurement disturbance in state-space form can be given by (Equations [16, 17]):

$$\dot{x} = A\,x + B\,u + w \quad [16]$$

$$y = C\,x + D\,u + \vartheta \quad [17]$$

Where, $x = [\omega_m \ \theta \ T_L]$, $u = \left[i_{q1}^*\right]$, $y = [\omega_m \ \theta]$ are the state vector, input and output of this 5-phase FOCPMSM drive system respectively and

$$A = \begin{bmatrix} -\frac{B_m}{J} & 0 & -\frac{1}{J} \\ 1 & 0 & 0 \\ 0 & 0 & 0 \end{bmatrix}, B = \begin{bmatrix} \frac{K_1\varphi_{m1}}{J} \\ 0 \\ 0 \end{bmatrix}, C = \begin{bmatrix} 1 & 0 & 0 \\ 0 & 1 & 0 \end{bmatrix} \text{ and } D = [0]$$

And the vectors w and ϑ are the sensor noise and measurement noise of the system respectively.

$$E[w] = 0, E[ww^T] = \text{cov}(w) = Q \quad [18]$$

$$E[\vartheta] = 0, E[\vartheta\vartheta^T] = \text{cov}(\vartheta) = R \quad [19]$$

$$E[w\vartheta] = 0 \quad [20]$$

The matrices Q and R in Equations [18, 19] represent the variances of system noise, w and measurement noise, ϑ respectively . Equation [20] gives the error between w and measurement noise, ϑ. Furthermore, Equations [14, 15] discretized using Forward Euler method and can be expressed in discrete-time state-space form by Equations [21-23] as given below:

$$\omega_m(t+1) = (1 - M_1T_1)\omega_m(t) + M_2T_1T_L(t) + M_3T_1i_{q1}^*(t) \quad [21]$$

$$\theta(t+1) = \theta(t) + \omega_m(t)T_1 \quad [22]$$

$$T_L(t+1) = T_L(t) \quad [23]$$

Similarly, state-space Equations [16] and [17] in discretized form can be stated by Equations [24, 25]:

$$x(t+1) = A_1\,x(t) + B_1\,u(t) + w \quad [24]$$

$$y(t) = C_1\,x(t) + D_1\,u(t) + \vartheta \quad [25]$$

Where,

$$A_1 = \begin{bmatrix} 1 - M_1T_1 & 0 & M_2T_1 \\ T_1 & 1 & 0 \\ 0 & 1 & 0 \end{bmatrix};\ B_1 = \begin{bmatrix} M_3T_1 \\ 0 \\ 0 \end{bmatrix};\ C_1 = \begin{bmatrix} 1 & 0 & 0 \\ 0 & 1 & 0 \end{bmatrix};\ \text{and}\ \ D_1 = [0]$$

It is to specifically mentioned here that this study does not include measurement noise, hence, $\vartheta \to 0$ taken hereafter.

Once the plant model including the white noise is developed, the Kalman filter minimizes the steady-state error covariance, P using its predicted state, $\hat{x}(t)$. Therefore, the error covariance, P, predicted state $\hat{x}(t)$,predicted output $\hat{y}(t)$ and $\frac{d\hat{x}}{dt}$ can be given as Equations [26-28]:

$$P = (\{x - \hat{x}\}\{x - \hat{x}\}^T) \quad [26]$$

$$[\hat{x}\ \hat{y}\ ] = [C_1\ I\ ]\hat{x} + [D_1\ 0\ ]u \quad [27]$$

$$\frac{d\hat{x}}{dt} = A_1\hat{x} + B_1u + L(y - C_1\hat{x} + D_1u) \quad [28]$$

Here, L is the Kalman gain matrix (Equation [29]) and is being solved with algebric Riccati Equation.

$$L = (PC_1^T + N)R^{-1} \quad [29]$$

The optimization function J(t), comprised of sum of square of plant input, u and difference of compared outputs at each sample time, t and this function is solved using the quadratic programming. The optimization function J(t) is given by Equation [30].

$$J(t) = \min\left\{\sum_{i=1}^{p}\ \left(y^*\left(t + \frac{i}{t}\right) - \hat{y}\left(t + \frac{i}{t}\right)\right)^2 + \mu\sum_{i=0}^{c-1}\ \left(u\left(t + \frac{i}{t}\right)\right)^2\right\} \quad [30]$$

In this Equation [30], the reference speed and weighting factor are given by y* and μ respectively. And, p and c are the predicted and control horizon.

Real-time Implementation

The research methodology of the current work and its real-time implementation is given in Figure 2. It can be seen from the figure that the nonlinear model of 5-phase FOCPMSM drive system with noise, comprising Equations [1-4, 10, 12] with MPC has been developed in MATLAB/SIMULINK environment. For development of the controller, the mentioned nonlinear model is converted into linear-time-invariant (LTI) model using system identification toolbox (SITB). The predicted horizon (p), control horizon (c) of controller and poles and zeros of the LTI model, till the fitness function has been adjusted equal to or greater than 90%.

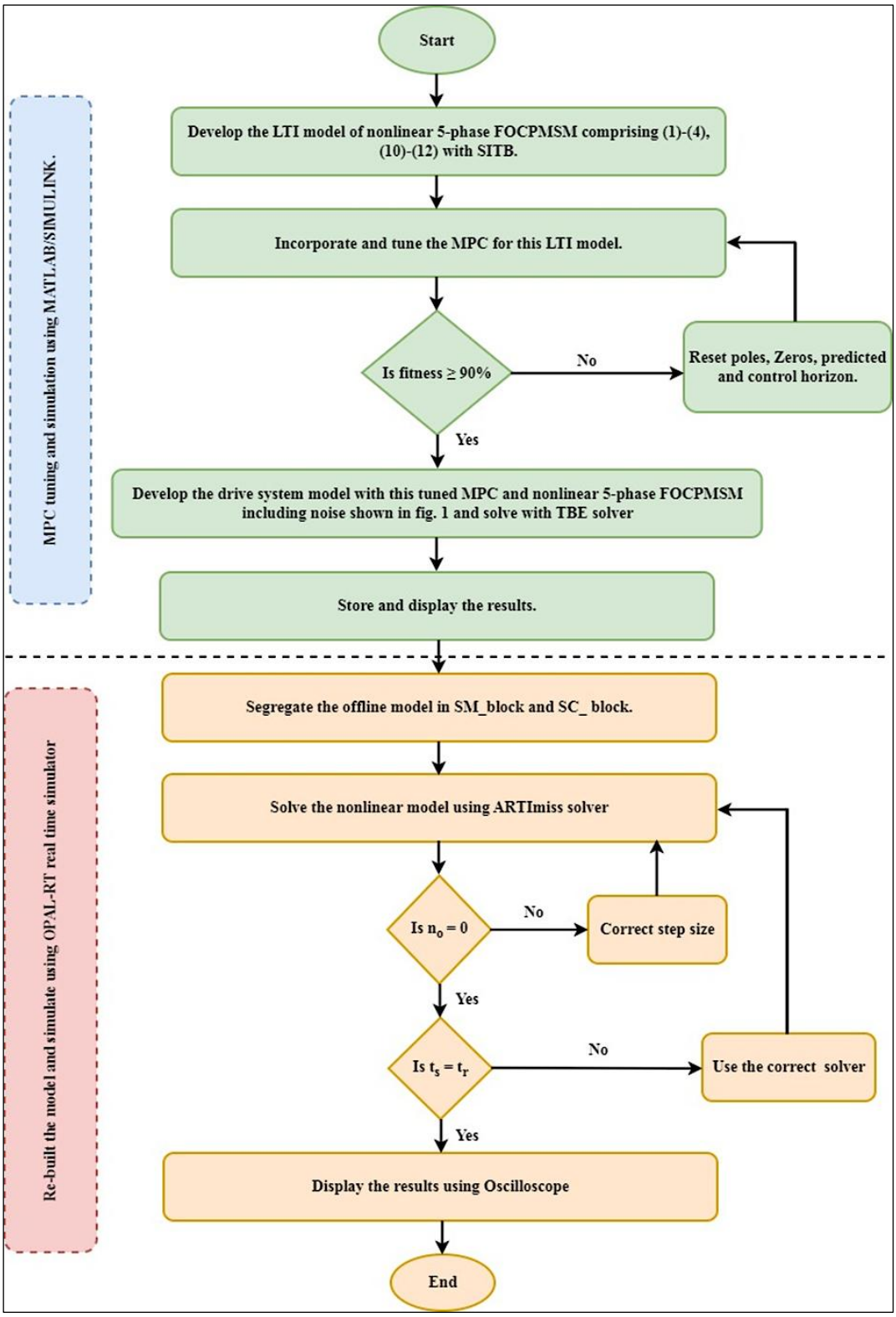

Figure 2: Flow Chart for Real-time Implementation

The trained MPC was put in nonlinear model and the whole model was simulated. It is noteworthy to mention that the signals generated are not real-time synchronized with real-time clock. Therefore, the offline model developed so far, was transformed into its online version using OPAL RT-4510 real time simulator. For this, the model is segregated into SM_ and SC_block. The overruns and execution time were adjusted to zero and real-time clock time respectively. Overruns has been reduced to zero using appropriate step-size, whereas, simulation time,ts has been made to real

clock time, tr with correct solver. The nonlinear model was simulated and the results have been stored with digital oscilloscope. The real-time experimental set-up with host PC, DB-37 connector, OPAL-RT 4510 simulator and digital oscilloscope are given in Figure 3.

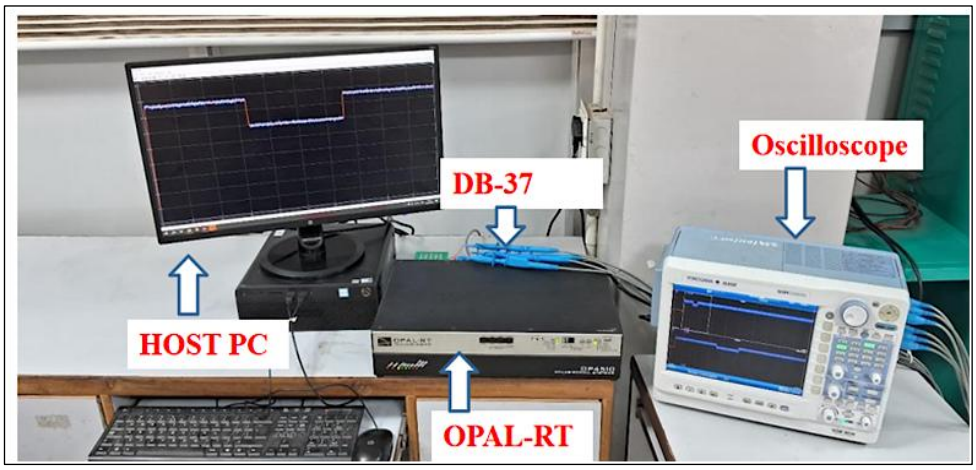

Figure 3: Pictorial-view of Real-time Experimental Set-up

Results and Discussion

The model of 5-phase PMSM drive system including mechanical sensor noise with proposed Kalman filter based model predictive controller shown in Figure 1, is developed using offline MATLAB/SIMULINK environment. It is compared in the same environment with conventional proportional-integral controller. The data for the drive system and the two controllers is given in Table 1. The parameters of both the controllers are achieved with hit-and-trial method.

Initially, the drive system is set to operate at 800 rpm for 0.15 seconds and then the drives speed is reduced to 400 rpm and continue to run for next 2 seconds. Then, the speed of the drive is increased to 600 rpm and runs at same speed for the remaining period. The reference load torque is 7 Nm for whole simulation period of 0.5 second.

Table 1: Parameters of Drive and Controllers

Machine and controllers	Units	Values
5-phase PMSM		
Power	Hp	6
Number of phases	-	5
Mechanical input , T_L	Nm	10
Stator phase resistance	Ohm	0.12
Armature inductance	H	1350e-6
Flux linkage	Wb	0.05
Moment of Inertia, J	Kg/m^2	0.002
Pole , P	-	2
Rotor flux position when theta = 0	-	90 degree behind phase A axis(modified Park)
PI controller		
Proportional constant (k_p)	-	20
Integral constant (K_i)	-	11
Kalman filter based MPC		
Prediction Horizon, p	-	12
Control Horizon, c	-	5
Sample time	Sec	5e-05

The non-linear differential Equations of the models developed in methodology section are discretized at a sample time of 5e-05 and solved using Tustin/Backward Euler (TBE) method.

Figures 4–9 present the comparative analysis of key variables for both controllers in the offline environment, followed by their corresponding online results in Figure 10.

Simulation Results in Offline Environment

The waveform traces of rotor speeds with both controllers are presented in Figure 4. It is evident that the initial peak-to-peak speed ripples at start up (zoom-1), during the first (zoom-2) and second speed changes (zoom-3) are 755-830, 320-450 and 570-650 rpm with the PI controller, whereas these values are 810-800, 390-400 and 605-595 rpm,

respectively, with the proposed controller. It is also noteworthy that the speed exhibits oscillatory behaviour even under steady-state conditions with the PI controller. However, this phenomenon is significantly reduced with MPC. Although, this speed ripple is comparable with latest technique, but without analysing of the effect of torque ripples (19). The simultaneous analyses of speed and torque are of paramount importance while designing these kinds of systems (24). Overall, the reduced speed oscillations demonstrate that the proposed Kalman-filter-based MPC effectively suppresses sensor-induced noise in rotor speed measurements and provides a more comprehensive dynamic evaluation framework, thereby offering improved robustness and practical relevance compared with existing approach (19).

From Equation [11], it is evident that the electromagnetic torque developed by the drive system is coupled with speed. Effective decoupling between these two parameters is crucial for enhancing the dynamics of any drive system for implementation in specific application (21). In this context, the controller plays a significant role. A critical analysis of the Figure 5 indicates that during each step change, i.e., at starting, during the first and second step changes, the initial peak-to-peak torque change is +80 to -40, -70 to +80 and +80 to -40 Nm with PI, whereas it is 0 to +80, 0 to -70 and 0 to +70 Nm, respectively, with the proposed controller. Notably, this torque is either positive or negative at each change with KF based MPC in comparison to PI. Therefore, the proposed controller puts fewer burdens on coupling of load and PMSM in industries where frequent load changes are prevalent.

Moreover, during steady-state, the peak-to-peak torque ripples are 50 to -30 and 0 to +20 Nm with PI and the proposed controller respectively, substantially reducing the torque ripples with the proposed controller in comparison to PI.

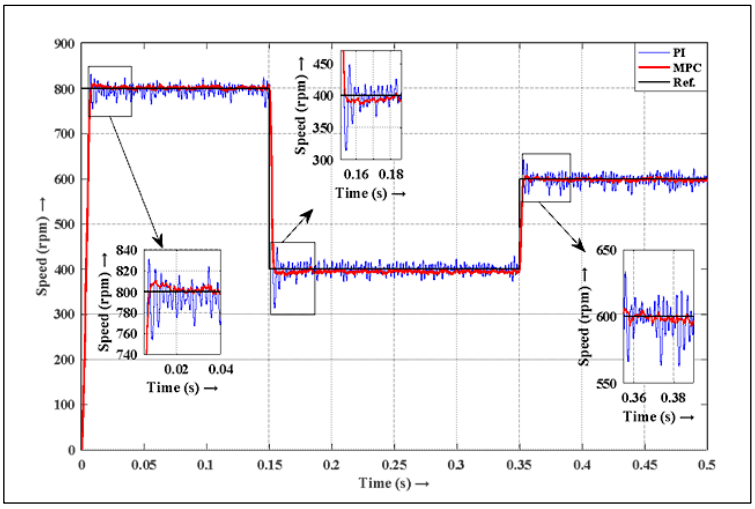

Figure 4: Speed Responses with Proportional-integral (PI) and Kalman-filter based Model-predictive-controller (MPC)

The torque-speed characteristics have been shown through a 2-D graph (Figure 6). It can be seen clearly that at 7 Nm of reference torque, the peak-to-peak torque is 25 and 110 Nm with proposed and conventional controller, respectively. Similar, enhanced performance at each step change in speed can be observed which confirms superior performance of Kalman filter based MPC at transient and steady-state condition in comparison to PI.

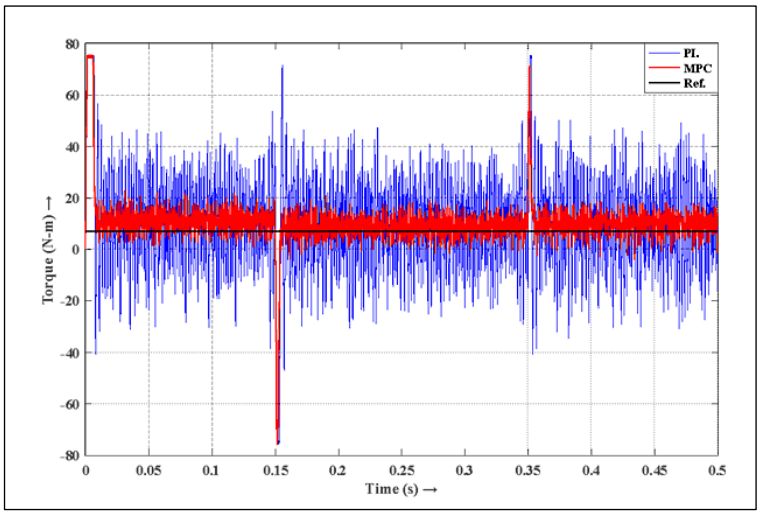

Figure 5: Torque Responses with Proportional-integral (PI) and Kalman-filter based Model-predictive-controller (MPC)

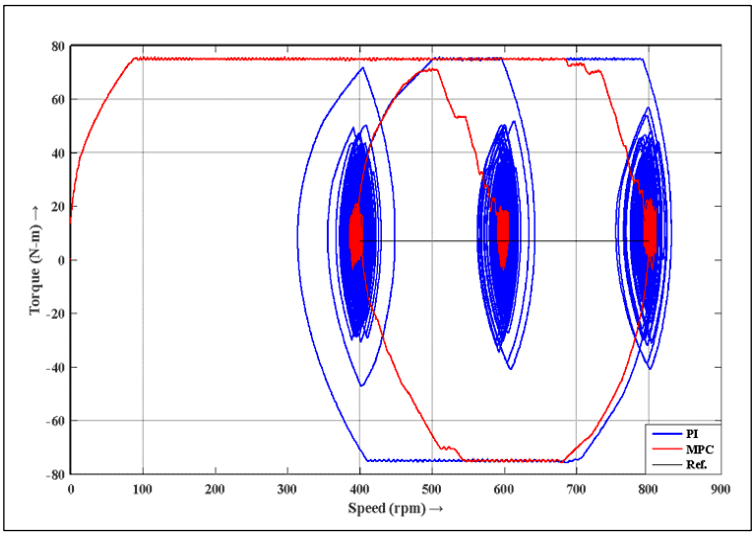

Figure 6: Speed-torque Responses with Proportional-integral (PI) and Kalman-filter based Model-predictive-controller (MPC)

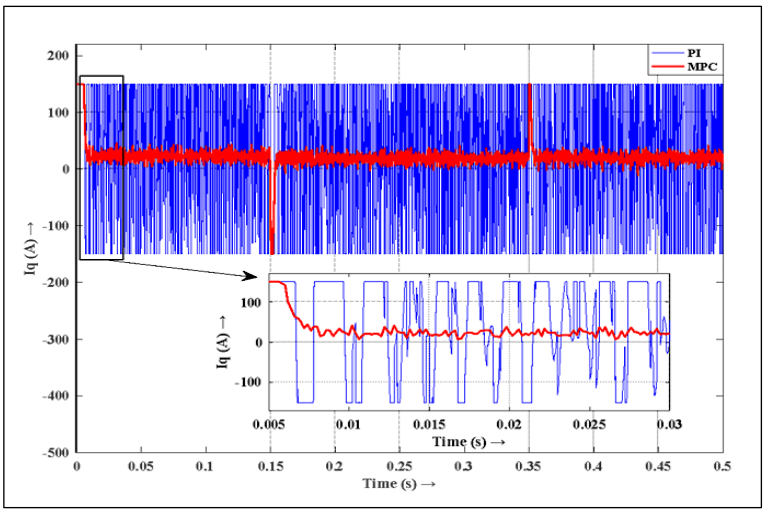

Figure 7: q-axis Current Responses with Proportional-integral (PI) and Kalman-filter based Model-predictive-controller (MPC)

It can be seen from Equation [10] that torque is directly proportional to reference q-axis current. Therefore, similar pattern of torque is being observed in reference q-axis current also. It is to be mentioned here that this reference current is being controlled with hysteresis controller. As even during steady-state period this current is changing from +150 to -150 amperes with PI (refer Figure 7). Whereas, this peak current is only during transient condition and that too either in positive side or on negative side. And during steady-state this current is 20 amperes (peak-to-peak) only. This is due to its inherent control approach (refer Equation [30]).

After d1-q1-d2-q2→αβ→abcde transformations, the actual 5-phase currents of the drive system can be obtained and out of all these, only phase 'a' current has been shown in Figure 8. It can be seen from this figure that during steady-state, the peak-to-peak current is 150 and 50 amperes with PI and proposed controller, respectively. This reduced peak-to-peak current with proposed controller, minimizes the copper losses and makes the drive system more efficient. Subsequently, the 1/3rd reduction in current results into reduced size of the copper wire, consequently reducing the size of the PMSM. Similarly, during starting period, the first peak-to-peak current is 270 and 210 amperes with PI and proposed controller respectively, reducing the size of the inverter.

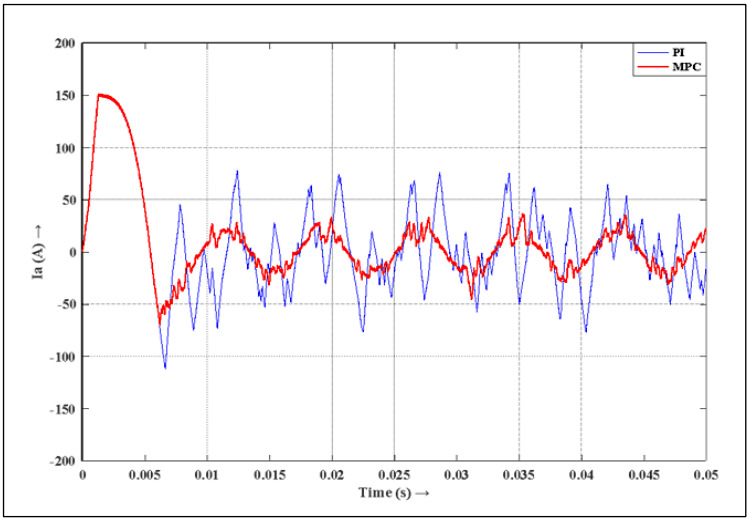

Figure 8: Phase 'a' Current Responses with Proportional-integral (PI) and Kalman-filter based Model-predictive-controller (MPC)

Table 2: Performance Indicators of Drive System with both the Controllers

Controllers	Changes	Performance Indicators (peak-to-peak) Change in speed(rpm) (Figures 4, 6)		Change in Torque (Nm) (Figures 5, 6)		Change in current (A) (Figure 8)	
		Transient	Steady-state	Transient	Steady-state	Transient	Steady-state
PI	Starting	75		120		270	
	First	130	40	150	80	150	150
	Second	80		120		150	
Kalman-filter based MPC	Starting	10		80		210	
	First	10	10	70	20	50	50
	Second	10		70		50	

Note: Proportional-integral (PI) and Kalman-filter based Model-Predictive-Controller (MPC)

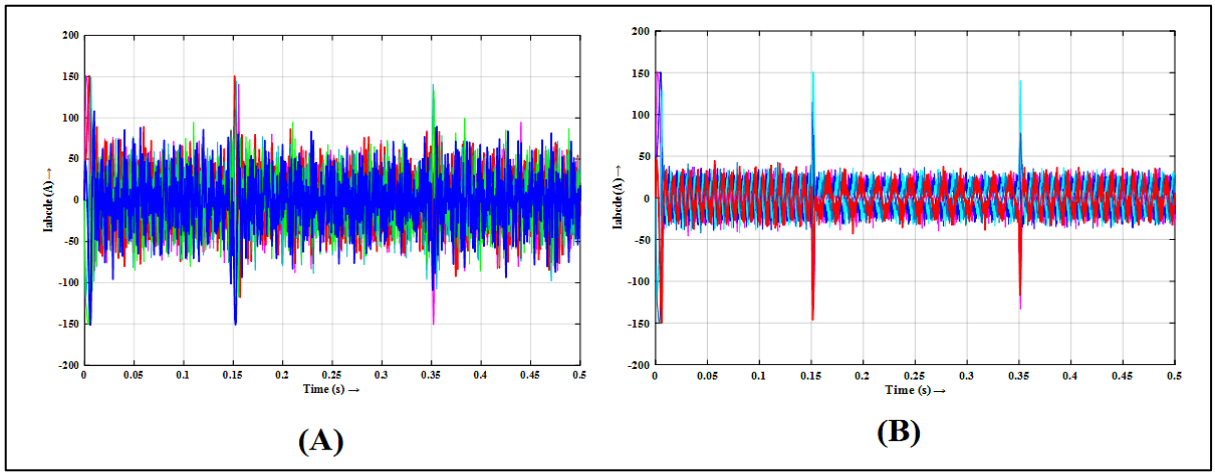

Figure 9: 5-Phase Current Responses with (A) Proportional-integral (PI) (B) Model-predictive-controller (MPC)

The comparative analysis of various performance indicators of drive system i.e. change in speed, electromagnetic torque and phase-a current with both the controllers are given in Table 2, which clearly indicates the enhanced performance of proposed controller.

Figure 9(A) and Figure 9(B) illustrate the actual 5-phase machine currents with the PI and proposed controller respectively. Comparison of these two also reveals that the currents have been reduced effectively with the proposed controller.

Overall, the offline results confirm that the proposed Kalman-filter-based MPC significantly outperforms the conventional PI controller in terms of speed, torque and current regulation. The controller effectively suppresses sensor-induced speed oscillations during startup, transients and steady-state operation, while simultaneously reducing torque ripple and improving speed–torque decoupling. This enhanced torque behavior leads to substantially lower q-axis and phase-current excursions, thereby reducing copper losses, thermal stress and inverter ratings. Unlike prior work that focuses primarily on speed regulation, the present study provides a holistic dynamic assessment, demonstrating the proposed controller's superior robustness and practical suitability for industrial PMSM drive applications (19).

Simulation Results in Online Environment

As discussed in research methodology section, the offline model is transformed into online model using the OPAL-RT 4510 real-time simulator. The real-time results of various variables like speeds, electromagnetic torques and q-axis current with both the controllers are given in Figure 10 (A-C) respectively. Figure 10(D) shows the phase-a current of the machine. Five-phase currents with PI and proposed controller are given in Figure 10(E, F) respectively. The upper part in these Figures illustrates the responses of variables for a long time-span whereas lower part shows the zoomed view of these variables for short duration. Although the response trends observed in the offline and online environments are qualitatively similar, practical implementation of controllers designed in offline settings poses significant challenges due to the generation of control signals that are not synchronized with real-time clocks. This issue is elucidated through the results summarized in Table 3. With a sampling time of 5e-05 sec, the offline simulation ensures high numerical accuracy; however, the fine discretization substantially increases computational time, leading to a mismatch with real-time execution requirements (25-27). The offline environment relies on conventional time-based explicit (TBE) solvers to handle the nonlinear dynamics of the five-phase FOC-PMSM drive, resulting in sequential computation. Consequently, the total simulation time reaches 950.5 s with 51,590 overruns and a model build-up time of 30.4 s. In contrast, the FPGA-based reconfigurable OPAL-RT platform employs the ARTimis solver with parallel processing, ensuring synchronization with real-time clocks and completely eliminating overruns. As a result, the effective computational burden is reduced to the required real-time value of one (27).

Table 3: Comparison of Simulating Environments

Environment	Sample time (sec)	Solver	Processing	Performance indicators of simulation environment				
				Build time (sec)	Simulation time (sec)	Real clock time(sec)	Number of overruns	Computation burden (ts/tr=1)
Offline	5e-05	TBE	Sequential	30.4	950.6	0.5	51590	1901.2
Online	3e-03	ARTimis	Parallel	140.8	0.5	0.5	0	1

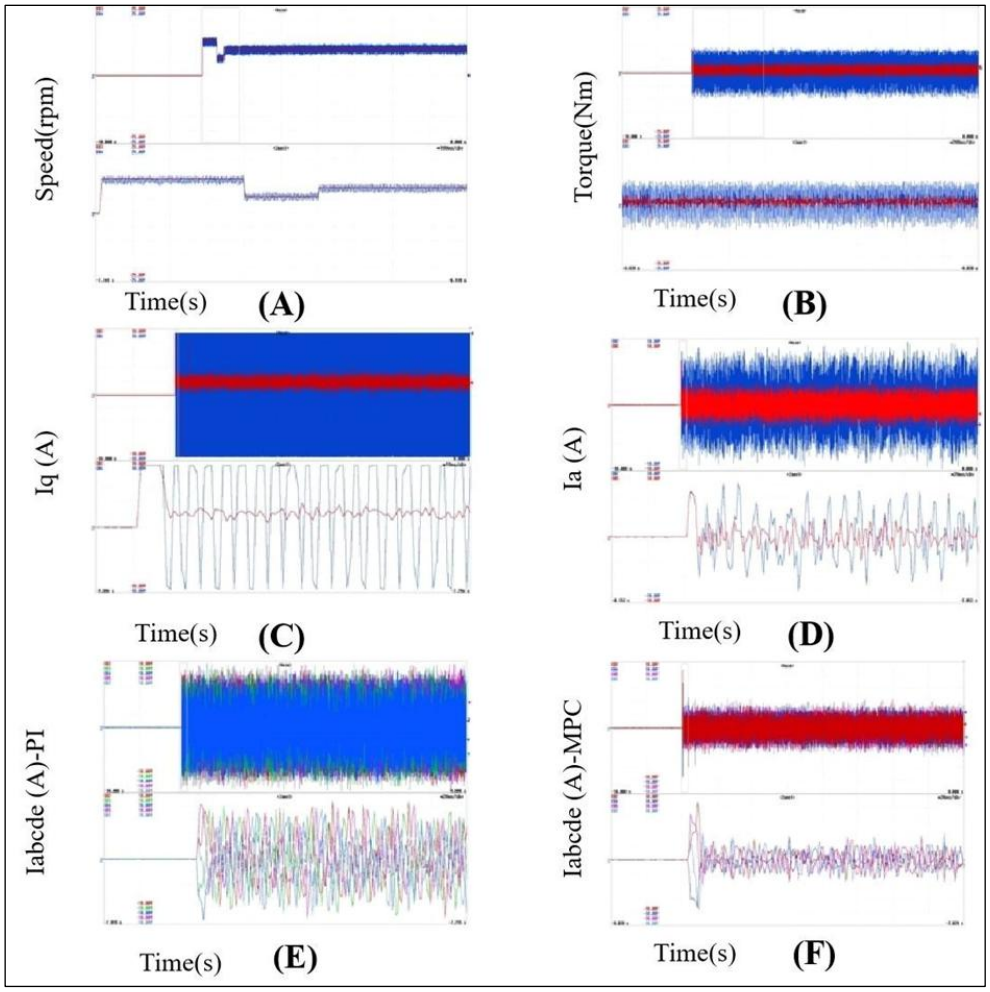

Figure 10: (A) Speed with both Controllers, (B) Torque with both Controllers, (C) q-axis Current with both Controllers (D) Phase 'a'currents with both Controllers (E) Five-phase Currents with Proportional-integral (PI), (F) Five-phase Currents with Model-predictive-controller (MPC)

Conclusion

A predictive control strategy augmented with Kalman-based state estimation has been investigated for a five-phase FOC-PMSM operating under noisy mechanical speed feedback. By embedding noise statistics directly into the control loop, the proposed KF-MPC framework improves both transient regulation and steady operating quality in a system characterized by strong cross-coupling and measurement uncertainty. Performance benchmarking against a PI-controlled drive reveals marked gains. Speed oscillations are constrained to approximately 10 rpm, corresponding to nearly a 75% attenuation relative to the baseline controller. Torque pulsations exhibit a comparable reduction, with steady-state variations compressed from the order of 80–150 Nm to below 70 Nm. Electrical current quality also improves substantially, with peak-to-peak ripple lowered by two-thirds (approx.), reflecting enhanced electromagnetic smoothness. Real-time assessment demonstrates the practical relevance of the method. While offline simulations suffer from severe computational overload and timing violations, the OPAL-RT implementation operates without overruns and maintains real-time synchronization.

These findings confirm the suitability of KF-MPC for noise-tolerant, high-performance multiphase PMSM drives. Future work will address adaptive noise modeling, robustness to parameter drift, effect of temperature on magnet and validation on physical drive hardware.

Abbreviations

FOC-PMSM: Field-oriented-controlled Permanent Magnet Synchronous Machine, KF: Kalman Filter, MPC: Model predictive control, PI: Proportional-Integral.

Acknowledgement

The author expresses thanks to the Ministry of Environment, Government of India, for awarding a grant under letter no. 17-11/2015-PN.1 for the provision of research facilities to UIET, Punjab University and Chandigarh for the Design Innovation Center.

Author Contributions

The author contributed solely in conceptualization, data curation, investigation, writing,-original draft, review and editing.

Conflict of Interest

The authors declare there is no conflict of interest.

Data Availability

The data supporting the findings of this study are included within the article. Additional datasets related to simulation models and experimental results are available from the corresponding author upon reasonable request.

Declaration of Artificial Intelligence (AI) Assistance

To improve the manuscript's grammar and clarity, AI-assisted tools such as Grammarly and ChatGPT were used.

Ethics Approval

This article does not encompass any studies involving human participants or animals conducted by the author.

Funding

There is no designated funding allocated for this work.

References

1. Wang F, He L, Rodriguez J. FPGA-based continuous control set model predictive current control for PMSM system using multistep error tracking technique. IEEE Trans Power Electron. 2020; 35(12):13455-13464. doi:10.1109/TPEL.2020.2984336
2. Wang Z, Chen J, Cheng M, Chau KT. Field-oriented control and direct torque control for paralleled VSIs fed PMSM drives with variable switching frequencies. IEEE Trans Power Electron. 2016; 31(3): 2417-2428. doi:10.1109/TPEL.2015.2437893
3. Tang Z, Akin B. A new LMS algorithm based deadtime compensation method for PMSM FOC drives. IEEE Trans Ind Appl. 2018;54(6):6472-6484. doi: 10.1109/TIA.2018.2853045
4. Ortega R, Praly L, Astolfi A, Lee J, Nam K. Estimation of rotor position and speed of permanent magnet synchronous motors with guaranteed stability. IEEE Transactions on Control Systems Technology. 2011; 19(3): 601–614. doi: 10.1109/TCST.2010.2047396
5. Yan Y, Yang J, Sun Z, Zhang C, Li S, Yu H. Robust speed regulation for PMSM servo system with multiple sources of disturbances via an augmented disturbance observer. IEEE/ASME Trans Mechatron. 2018; 23(2):769-780.
6. Islam R, Husain I. Analytical model for predicting noise and vibration in permanent-magnet synchronous motors. IEEE Trans Ind Appl. 2010; 46(6):2346-2354. doi:10.1109/ECCE.2009.5316074
7. Wang S, Li H. Effects of rotor skewing on the vibration of permanent magnet synchronous motors with elastic-plastic stator. IEEE Trans Energy Convers. 2022; 37(1): 87-96. doi: 10.1109/TEC.2021.3100285
8. Wang YS, Guo H, Yuan T, Ma LF, Wang C. Electromagnetic noise analysis and optimization for permanent magnet synchronous motor used on electric vehicles. Eng Comput. 2021; 38(2): 699-719. https://doi.org/10.1108/EC-02-2020-0070
9. Sarsembayev B, Suleimenov K, Do TD. High order disturbance observer based PI-PI control system with tracking anti-windup technique for improvement of transient performance of PMSM. IEEE Access. 2021; 9: 66323-66334. doi:10.1109/ACCESS.2021.3074661
10. Ding S, Hou Q, Wang H. Disturbance-observer-based second-order sliding mode controller for speed control of PMSM drives. IEEE Trans Energy Convers. 2023; 38(1): 100-110. doi:10.1109/TEC.2022.3188630
11. Li S, Yang J, Chen WH, Chen X. Generalized extended state observer based control for systems with mismatched uncertainties. IEEE Trans Ind Electron. 2012; 59(12): 4792-4802. doi:10.1109/TIE.2011.2182011
12. Ahmad S, Ali A. On active disturbance rejection control in presence of measurement noise. IEEE Trans Ind Electron. 2022; 69(11): 11600-11610. doi:10.1109/TIE.2021.3121754
13. Zuo YF, Zhu XY, Li Q, Zhang C, Du Y, Xiang ZX. Active disturbance rejection controller for speed control of electrical drives using phase-locking loop observer. IEEE Trans Ind Electron. 2019; 66(3): 1748-1759. doi: 10.1109/TIE.2018.2838067
14. Hou QK, Ding SH. Finite-time extended state observer based super-twisting sliding mode

controller for PMSM drives with inertia identification. IEEE Trans Transp Electrif. 2022; 8(2): 1918-1929. doi:10.1109/TTE.2021.3123646
15. Hao Z, Yang Y, Gong Y, *et al.* Linear-Nonlinear active disturbance rejection switching control for permanent magnet synchronous motors. IEEE Trans Power Electron. 2021; 36(8): 9334–9347. https://doi.org/10.3390/s22249611
16. Xia C, Wang M, Song Z, Liu T. Robust model predictive current control of three-phase voltage source PWM rectifier with online disturbance observation. IEEE Trans Ind Inf. 2012; 8(3): 459-471. doi:10.1109/TII.2012.2187912
17. Zhang X, Hou B, Mei Y. Deadbeat predictive current control of permanent-magnet synchronous motors with stator current and disturbance observer. IEEE Trans Power Electron. 2017; 32(5): 3818-3834. doi:10.1109/TPEL.2016.2592534
18. Song Z, Zhou F, Zhang Z. Parallel-observer-based predictive current control of permanent magnet synchronous machines with reduced switching frequency. IEEE Trans Ind Inf. 2019; 15(12): 6457-6467. doi: 10.1109/TII.2019.2910842
19. Hou Q, Xu S, Zuo Y, Wang H, Sun J, Lee CHT, Ding S. Enhanced active disturbance rejection control with measurement noise suppression for PMSM drives via augmented nonlinear extended state observer. IEEE Transactions on Energy Conversion, 2024; 39(1): 287–299. doi:10.1109/TEC.2023.3323310
20. Yang Z, Miao C, Sun X, Guo D. Robust Model Predictive Torque Control of Interior PMSM Drives With Kalman-Based Disturbance Observer. IEEE Transactions on Transportation Electrification. 2024; 10(2): 2434-2444. https://doi.org/10.1109/TTE.2023.3296684
21. Casadei D, Profumo F, Serra G, Tani A. FOC and DTC: two viable schemes for induction motors torque control. IEEE Trans Power Electron. 2002; 17(5): 779–787. doi:10.1109/TPEL.2002.802183
22. Parsa L, Toliyat HA. Five-phase permanent-magnet motor drives. IEEE Trans Ind Appl. 2005; 41(1): 30-37. doi:10.1109/ESTS.2005.1524702
23. Tao T, Zhao W, He Y, Cheng Y, Saeed S, Zhu J. Enhanced fault tolerant model predictive current control for a five-phase PM motor with continued modulation. IEEE Trans Power Electron. 2021; 36(3): 3236-3246. doi:10.1109/TPEL.2020.3018302
24. Pahwa V, Kumar D, Bhushan P, Verma YP. Improved dynamics of coupled 5-phase vector-controlled PMSM drive system with model-predictive-controller. Arab J Sci Eng. 2025; 50(21): 17347-17367. doi: 10.1007/s13369-024-09933-3
25. Faruque MO, Strasser T, Lauss G, *et al.* Real-time simulation technologies for power systems design, testing and analysis. IEEE Power Energy Technol Syst J. 2015; 2(2): 63-73. doi:10.1109/JPETS.2015.2427370
26. Song X, Cai H, Jiang T, *et al.* Research on Performance of Real-Time Simulation Based on Inverter-Dominated Power Grid. IEEE Access. 2021; 9: 1137–1153. doi:10.1109/ACCESS.2020.3016177
27. Karad SG, Thakur R, Alotaibi MA, *et al.* Optimal design of fractional order vector controller using hardware-in-loop (HIL) and OPAL-RT for wind energy system. IEEE Access. 2024; 12: 35033–35047. doi:10.1109/ACCESS.2024.3357504
28. Liang X, Talha M, Pannell J, Su H, Bowes A. A novel OPAL-RT real-time simulator-based experimental approach to study open-switch faults of interfacing inverters of renewable distributed generation in microgrids. IEEE Transactions on Industry Applications. 2025; 61(3): 5218–5229. doi:10.1109/TIA.2025.3536426

How to Cite: Pahwa V. Noise Mitigation of a 5-phase Field-oriented-controlled Permanent Magnet Synchronous Machine Drive System Using Kalman Filter-based Model-predictive-controller. Int Res J Multidiscip Scope. 2026; 7(2): 764-777. DOI: 10.47857/irjms.2026.v07i02.08248